A NEW EFFICIENT METHOD FOR CALCULATION AND SUPPRESSION OF SIMULTANEOUS SWITCHING NOISE WITH THE TIME-DOMAIN IMPEDANCE FUNCTION FOR HIGH-SPEED CIRCUIT DESIGN

T.-H. Ding, Y.-S. Li, X. Yan, and Y.-Z. Qu

School of Electronic Engineering
Xidian University
No. 2 South Taibai Road, Xi'an, Shaanxi 710071, China

Abstract—In this paper, a new method is proposed to calculate the simultaneous switching noise (SSN) in order to reduce the complexity of SSN circuit models and computational burden, which is based on the rational function (RF) in time domain. The time-domain impedance function of a power delivery network (PDN) is calculated by approximating the impedance frequency response of a PDN with a rational function, and the SSN is calculated based on switching current characteristics. It is also found that the SSN can be suppressed through adjusting the period of time-domain impedance function and switching current. Compared with the simulated results and measured results, the performance of the new method for calculating and suppressing the SSN is verified, and the simulation time of SSN is reduced effectively.

1. INTRODUCTION

With the trend of the integrated circuit (IC) technology scaled downward to smaller and faster transistors, digital, analog, radio frequency and other function circuits are integrated into one package or printed circuit board (PCB), which results in increasing current [1]. Simultaneous switching noise (SSN) has become one of the major difficulties in the design of high-speed digital circuit systems with even faster edge rates, lower voltage levels and higher integrations. The SSN is mainly attributes to three reasons, inductance of non-ideal signal path, mutual inductive coupling of PDNs and power supply compression, so SSN is also known as power/ground bounce noise

or delta-I noise. If the SSN exceeds the noise margin, the IC may experience a functional failure. Hence, the target impedance should be met to maintain the proper supply voltage when transistors switch.

To ensure the success in the design of high-speed circuits, equivalent circuit extraction techniques [2–8] are adopted to model the behavior of interconnections at high frequencies. How to develop appropriate equivalent networks with wideband features, and at the same time possess rather complicated coupling schemes, is a very challenging task by the conventional approaches [9–15]. The modeling methods have been discussed in many papers, the partial equivalent electric circuit (PEEC) method is widely used to model complex three-dimensional structures, which has also been extended with retardation to provide a full-wave solution, but it has a limited bandwidth because the distributed nature of the capacitance is not taken into account at higher frequencies. The transmission matrix method (TMM) uses a fast method of computing the port-to-port behavior of planes based on the transmission matrix (or ABCD matrix) of each column of unit cells. The frequency-domain finite-difference method (FDM) and the time-domain finite-difference time-domain (FDTD) method could also be used to get time and frequency domain results [16, 17].

One of the challenges of PDN design is to provide clean power to electronics when a surge current occurs, so the suppression of SSN on a multilayer PCB is a critical task in system design to ensure signal integrity and to reduce the risk of EMI problems. Many studies have focused on the suppression of noise transmission, such as embedded capacitors [18, 19] are commonly used in the power bus to mitigate the high frequency noise due to their lower inductance. Power islands [20, 21] are used to isolate devices that put noise on a power bus from devices that may be susceptible to power bus noise. Lossy components are introduced to eliminate resonances by increasing the component loss [22] and electromagnetic band-gap (EBG) structures [23, 24] are proposed to suppress the SSN in GHz range because of their high-impedance planes.

The investigation of SSN is mainly done in frequency domain, so the transient response of SSN is neglected due to transient characteristics of time-domain impedance and switching current are not considered. In this paper, a new method is proposed to calculate and suppress the SSN in order to take the transient response of SSN into account in time domain. The time-domain impedance function of a PDN is obtained by approximating the impedance frequency response of a PDN with a rational function and the SSN is calculated based on switching current characteristics. The periodic characteristics of the time-domain impedance function are also discussed in detail, and

it is found that the SSN can be suppressed through adjusting the periods of time-domain impedance function and switching current. The performance of the new method is verified with the results of lumped, distributed PDN models and measured results, and the accuracy of SSN calculation and efficiency of SSN suppression are validated.
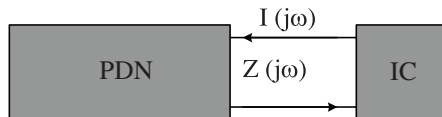
2. RATIONAL APPROXIMATION OF THE IMPEDANCE FREQUENCY RESPONSE

$$Z\left(j\omega\right) \le Z_T = \frac{V_{dd} \times ripple}{I_{\text{average}}} \tag{1}$$

The schematic diagram of SSN suppression and transmission is shown in Fig. 1, where PCBs, voltage regulator modules (VRM) and many types of capacitors are included in the PDN, $Z\left(j\omega\right)$ is the frequency-domain impedance function of the PDN, and $I\left(j\omega\right)$ is the frequency-domain function of switching current. As shown in Equation (1), $Z\left(j\omega\right)$ should be lower than the target impedance for noise voltage less than the allowed ripple in high-speed circuit design [25], but the transient characteristics of impedance and switching current are not considered, so an improper design may be produced [26–28]. The SSN waveform couldn't be directly calculated with $Z\left(j\omega\right)$ because that the frequency-domain impedance function couldn't be derived from the circuit model which includes the power/ground planes and on which many types of capacitors are in time domain. So the frequency-domain impedance is approximated with a rational function, and time-domain impedance can be expressed with the exponential functions by inverse Laplace transformation.

The PDN is supposed as a black box model, the goal is to construct a function that captures the impedance frequency response between the ports [29]. This function can be written as

$$Z\left(s\right) = c + \sum_{n=1}^{N} \frac{k_n}{s - p_n} \tag{2}$$

Figure 1. Schematic diagram of the SSN suppression and transmission.

where s is the Laplace variable, p_n is the n-th pole, k_n is the residue corresponding to the n-th pole, N is the order of the rational function, and c is a constant. Multiplying the Equation (2) with an weighting function $\sigma(s) = 1 + \sum\limits_{n=1}^{N} \frac{\tilde{k}_n}{s - \bar{p}_n}$, Equation (2) is equivalent to

$$\sigma(s) Z(s) = c + \sum_{n=1}^{N} \frac{k_n}{s - \bar{p}_n} \tag{3}$$

Substitute $\sigma(s) = 1 + \sum\limits_{n=1}^{N} \frac{\tilde{k}_n}{s - \bar{p}_n}$ into (3), leads to

$$c + \sum_{n=1}^{N} \frac{k_n}{s - \bar{p}_n} = \left[1 + \sum_{n=1}^{N} \frac{\tilde{k}_n}{s - \bar{p}_n} \right] Z(s) \tag{4}$$

Equation (4) can be rewritten as

$$Ax = b \tag{5}$$

where

$$A = \begin{bmatrix} & & & \vdots & & & \\ \frac{1}{s_k - p_1} & \cdots & \frac{1}{s_k - p_N} & 1 & \frac{-Z(s_k)}{s_k - p_1} & \cdots & \frac{-Z(s_k)}{s_k - p_N} \\ & & & \vdots & & & \end{bmatrix},$$

$$x = \begin{bmatrix} k_1 \ldots k_N c \tilde{k}_1 \ldots \tilde{k}_N \end{bmatrix}^T,$$

$$b = [Z(s_1) \ldots Z(s_k) \ldots Z(s_m)]^T$$

s_k is the k-th sample of frequency. With enough frequency samples, the rank of A is larger than the number of the element x, Equation (5) can be solved as an overdetermined function using the least-squares solution. $Z(s)$ can be obtained as

$$Z(s) = \frac{\prod\limits_{n=1}^{N} (s - z_n)}{\prod\limits_{n=1}^{N} (s - \tilde{z}_n)} \tag{6}$$

The poles of $Z(s)$ are substituted with the zeros of $\sigma(s)$, $\tilde{z}_n$, the poles converge to constant values by iteration. Substituting the new poles into Equation (2), a new matrix Equation (7) can be generated and solved with samples of frequency, where the unknown parameters

contains the coefficients c and k_n as

$$
\begin{bmatrix}
 & \vdots & \\
1 & \frac{1}{s_k - \tilde{z}_1} \cdots \frac{1}{s_k - \tilde{z}_N} \\
 & \vdots &
\end{bmatrix}
\begin{bmatrix}
c \\
k_1 \\
\vdots \\
k_n
\end{bmatrix}
=
\begin{bmatrix}
Z(s_1) \\
\vdots \\
\vdots \\
Z(s_n)
\end{bmatrix}
\tag{7}
$$

The frequency-domain impedance can be approximated with a rational function as Equation (2), and passivity enforcement is realized. So the time-domain impedance function can be easily obtained by inverse Laplace transformation and the time-domain waveform of SSN can be calculated based on the characteritics of switching current.

3. CALCULATION OF THE SIMULTANEOUS SWITCHING NOISE

The frequency-domain impedance approximated with a rational function can be rewritten as Equation (8), the n-th poles $p_{nr} - jp_{ni}$, $p_{nr} + jp_{ni}$ and corresponding residues $k_{nr} - jk_{ni}$, $k_{nr} + jk_{ni}$ are complex conjugate pairs, b_m is the m-th real pole and a_m is the corresponding real residue.

$$
Z(s) = c + \sum_{m=1}^{M} \left(\frac{a_m}{s - b_m} \right) + \sum_{n=1}^{N} \left(\frac{k_{nr} + jk_{ni}}{s - p_{nr} - jp_{ni}} + \frac{k_{nr} - jk_{ni}}{s - p_{nr} + jp_{ni}} \right) \tag{8}
$$

Based on the complex conjugate characteristics, Equation (8) can be rewritten as

$$
Z(s) = c + \sum_{m=1}^{M} \left(\frac{a_m}{s - b_m} \right) + \sum_{n=1}^{N} \left(\frac{2k_{nr}(s - p_{nr}) - 2k_{ni}p_{ni}}{(s - p_{nr})^2 + p_{ni}^2} \right) \tag{9}
$$

By inverse Laplace transformation, the time-domain impedance function can be obtained as

$$
z(t) = c\delta(t) + \sum_{m=1}^{M} a_m e^{b_m t} + \sum_{n=1}^{N} 2k_{nr} e^{p_{nr} t} \cos(p_{ni} t) \varepsilon(t)
$$

$$
- \sum_{n=1}^{N} 2k_{ni} e^{p_{nr} t} \sin(p_{ni} t) \varepsilon(t) \tag{10}
$$

With $\theta = \arccos \frac{k_{nr}}{\sqrt{(k_{nr}^2 + k_{ni}^2)}}$, Equation (10) can be rewritten as

$$
z(t) = c\delta(t) + \sum_{m=1}^{M} a_m e^{b_m t} + 2 \sum_{n=1}^{N} e^{p_{nr} t} \sqrt{(k_{nr}^2 + k_{ni}^2)} \cos(p_{ni} t + \theta) \varepsilon(t)
\tag{11}
$$

The time-domain waveform of SSN could be calculated as

$$v(t) = \left[c\delta(t) + \sum_{m=1}^{M} a_m e^{b_m t} + 2 \sum_{n=1}^{N} e^{p_{nr}t} \sqrt{\left(k_{nr}^2 + k_{ni}^2\right)} \cos(p_{ni}t+\theta)\varepsilon(t) \right] * i(t)$$

(12)

The digital signal voltage and switching current waveforms are shown in Fig. 2, the width of switching current is the rise/fall time of the digital signal, 10%–20% of the digital signal period. For GHz digital signals, the width of switching current is in the order of 10^{-1} ns, and the main resonant period is larger than 1ns for typical PDNs. So the switching current could be seen as an impulse signal with a limited magnitude if the main resonant period of the PDN is large enough compared with the current pulse width. Because of $\int_{-\infty}^{\infty} \delta(t)dt = 1$, the integral of the switching current pulse can be obtained as

$$\int_{-\infty}^{\infty} i(t)dt = S \int_{-\infty}^{\infty} \delta(t)dt$$

(13)

where S is the area of current pulse, so the switching current pulse can be substituted with $i(t) = S\delta(t)$, the time-domain waveform of SSN can be calculated as

$$v(t) = ci(t) + S\left[\sum_{m=1}^{M} a_m e^{b_m t} + 2 \sum_{n=1}^{N} e^{p_{nr}t} \sqrt{\left(k_{nr}^2 + k_{ni}^2\right)} \cos\left(p_{ni}t+\theta\right)\varepsilon(t) \right]$$

(14)

The range of the frequency-domain impedance needed to be considered is the bandwidth (BW) of the current pulse [30], which could be
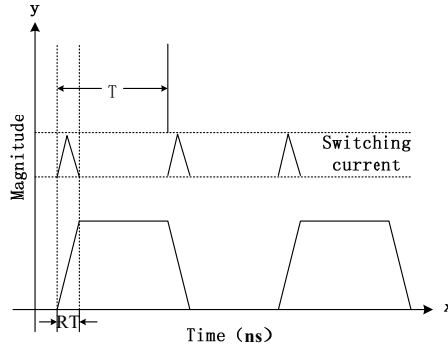
Figure 2. Digital signal voltage and switching current waveforms.

calculated with the rise time (rt) of current pulse as

$$BW = \frac{0.35}{rt} \tag{15}$$

The switching current is periodic, and the period of digital signals is T, so the periodic SSN can be gotten as

$$v(t) = c\sum_{l=0}^{\infty} i(t - lT) + S\sum_{l=0}^{\infty} \left[\sum_{m=1}^{M} a_m e^{b_m(t-lT)} \right.$$
$$\left. + 2\sum_{n=1}^{N} e^{p_{nr}t} \sqrt{\left(k_{nr}^2 + k_{ni}^2\right)} \cos\left(p_{ni}(t-lT) + \theta\right) \varepsilon(t-lT) \right] \tag{16}$$

It is found that the SSN is periodic accumulation of the time-domain impedance waveform. For real poles and residues, the magnitude of noise is determined by residues a_m, and the damping characteristic is determined by poles b_m. For complex-conjugate poles and residues the magnitude of noise is determined by the real parts and imaginary parts of residues k_{nr} and k_{ni}. The damping in transient response is introduced by the real parts of poles p_{nr}. The period of the noise is determined by the imaginary parts of poles p_{ni}. All characteristic parameters of time-domain waveform are included in Equation (16), so the noise of PDNs could be expressed with it.

In real circuit system, the PDN is a multi-port system which could be represented by a Z matrix, as Equation (17), Z_{ii} is the self-impedance of the i-th port, Z_{ij} is the transfer-impedance between the j-th port and the i-th port.

$$[Z] = \begin{bmatrix} Z_{11} & \cdots & Z_{1k} \\ \vdots & \ddots & \vdots \\ Z_{k1} & \cdots & Z_{kk} \end{bmatrix} \tag{17}$$

The elements of Z matrix could be approximated with rational functions respectively, so Equation (17) can be rewritten as

$$[Z] = \begin{bmatrix} c_{11} + \sum_{n=1}^{N_{11}} \frac{k_n^{11}}{s-p_n^{11}} & \cdots & c_{1k} + \sum_{n=1}^{N_{1k}} \frac{k_n^{1k}}{s-p_n^{1k}} \\ \vdots & \ddots & \vdots \\ c_{k1} + \sum_{n=1}^{N_{k1}} \frac{k_n^{k1}}{s-p_n^{k1}} & \cdots & c_{kk} + \sum_{n=1}^{N_{kk}} \frac{k_n^{kk}}{s-p_n^{kk}} \end{bmatrix} \tag{18}$$

where p_n^{ij} is the n-th pole of Z_{ij}, k_n^{ij} is the residue corresponding to the n-th pole, N_{ij} is the order of the corresponding rational function, and

c_{ij} is the corresponding constant. So the SSN of the i-th port could be calculated as

$$v_i(t) = z_{i1}(t) * i_1(t) + \ldots + z_{ij}(t) * i_j(t) + \ldots + z_{ik}(t) * i_k(t) \quad (19)$$

where $i_j(t)$ is the switching current of the j-th port, $z_{ij}(t)$ is the inverse Laplace transformation of $Z_{ij}(s)$, so the SSN of a multi-port PDN could also be calculated with the proposed method.

4. ANALYSIS OF THE TIME-DOMAIN IMPEDANCE FUNCTION

4.1. Network Synthesis

The pole-residue representation of a frequency-domain impedance function can be represented by electric networks consisting of resistors, inductors and capacitors. As shown in Fig. 3, the rational function with real poles and residues could be represented with RC networks, and the rational function with complex-conjugate poles and residues could be represented with RLC networks

where

$$R_{real} = \frac{-a_m}{b_m} \quad (20)$$

$$C_{real} = \frac{1}{a_m} \quad (21)$$

$$R_{1complex} = \frac{-2p_{nr}k_{nr}^3 - 2k_{nr}^2 k_{ni}p_{ni}}{p_{ni}^2 k_{nr}^2 + p_{ni}^2 k_{ni}^2} \quad (22)$$

$$R_{2complex} = \frac{2k_{nr}^2}{k_{ni}p_{ni} - k_{nr}p_{nr}} \quad (23)$$

$$C_{complex} = \frac{1}{2k_{nr}} \quad (24)$$
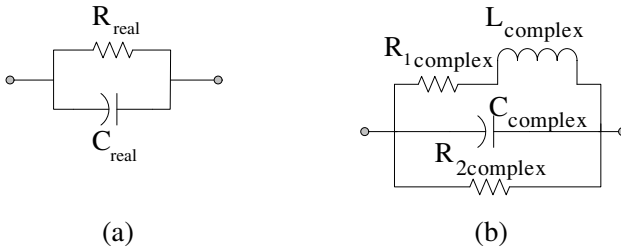
Figure 3. Electric networks of rational functions. (a) Real poles and residues. (b) Complex poles and residues.

$$L_{complex} = \frac{2k_{nr}^3}{p_{ni}^2 k_{nr}^2 + p_{ni}^2 k_{ni}^2} \tag{25}$$

So the resonant period for the electric networks of complex poles and residues could be calculated as

$$T_{resonance} = 2\pi / \sqrt{p_{ni}^2 - p_{nr}^2 - 2p_{nr}p_{ni}k_{ni}/k_{nr}} \tag{26}$$

With $p_{ni}^2 \gg p_{nr}^2 + 2p_{nr}p_{ni}k_{ni}/k_{nr}$, the resonant period can be simplified as

$$T_{resonance} = 2\pi / p_{ni} \tag{27}$$

It is found that the resonant period is consistent with the period of the time-domain impedance function with $p_{ni}^2 \gg p_{nr}^2 + 2p_{nr}p_{ni}k_{ni}/k_{nr}$. The PDN can be represented with series RLC and RC networks. For electric networks of real poles and residues, the lower frequency-domain impedance of the PDN can be achieved by smaller R_{real} and larger C_{real}, which is realized by reducing a_m and enlarging b_m, and for electric networks of complex-conjugate poles and residues, the lower frequency-domain impedance can be obtained by reducing $R_{1complex}$, $R_{2complex}$, $L_{complex}$ and enlarging $C_{complex}$, which imply smaller k_{nr} and lower time-domain impedance, so it is concluded that the lower frequency-domain impedance of electric networks can be realized by reducing the time-domain impedance through smaller parasitic inductance and larger decoupling capacitance.

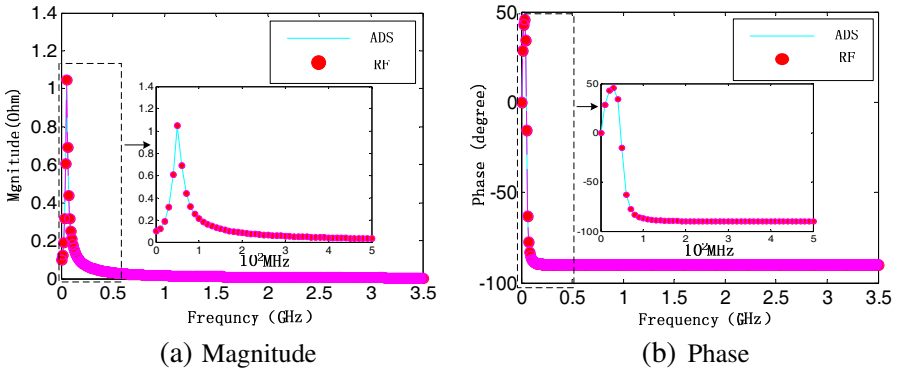## 4.2. Analysis of the Time-domain Impedance Function with the Single Resonance Circuit Model

The SSN suppression circuit can be simplified to a single resonance circuit model, as shown in Fig. 4, which consists of a $0.1\,\Omega$ resistor, a $1\,\text{nH}$ inductor, a VRM with DC voltage $V_{dd} = 3.3\,\text{V}$, a variable capacitor of $C = 10\,\text{nF}$ and $C = 20\,\text{nF}$. The time-domain impedance waveform could be obtained by an impulse signal exciting the circuit. The used current pulse in ADS has a rise/fall time of $0.1\,\text{ns}$, an
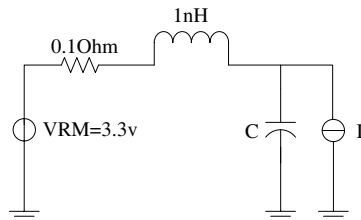

Figure 4. Single resonance circuit model.

amplitude of 10^{10} A, which results in $S = 1$. So the bandwidth of the frequency-domain impedance should be considered is 3.5 GHz, and the current pulse could be seen as impulse signal compared to the resonant period of the circuit. The simulated frequency-domain impedance of ADS and the approximated results with rational functions are shown in Fig. 5 and Fig. 6. The obtained poles and residues of $C = 10$ nF are $-5 \times 10^7 \pm j3.1225 \times 10^8$ and $5 \times 10^7 \mp j8.006 \times 10^6$, and the constant c is 3.1104×10^{-17}; the obtained poles and residues of $C = 20$ nF are $-5 \times 10^7 \pm j2.1794 \times 10^8$ and $2.5 \times 10^7 \mp j5.735 \times 10^6$ respectively, and the constant c is 3.1106×10^{-17}.

The simulated time-domain impedance function waveforms of ADS and the proposed method are shown in Fig. 7, a good agreement is achieved. It is found that the magnitude of the time-domain impedance of $C = 20$ nF is reduced effectively due to larger capacitance, which also results in reduced residues and lower frequency-domain impedance.

(a) Magnitude   (b) Phase

Figure 5. Input impedance of the PDN with $C = 10$ nF.

(a) Magnitude   (b) Phase
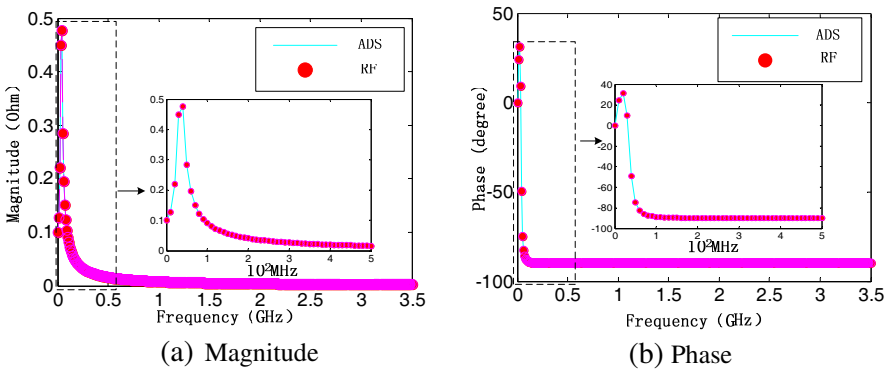
Figure 6. Input impedance of the PDN with $C = 20$ nF.
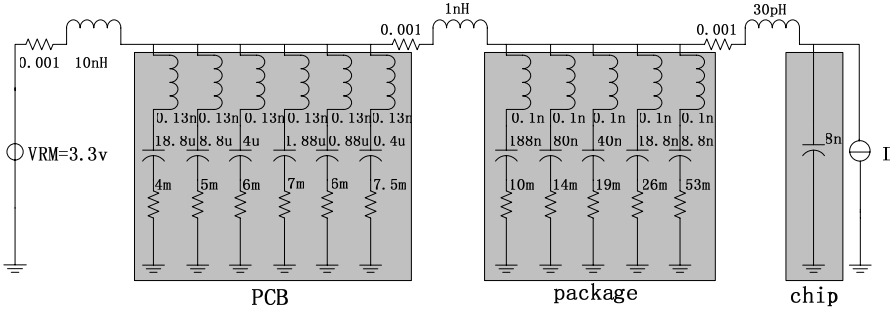
(a) C=10 nF   (b) C=20 nF
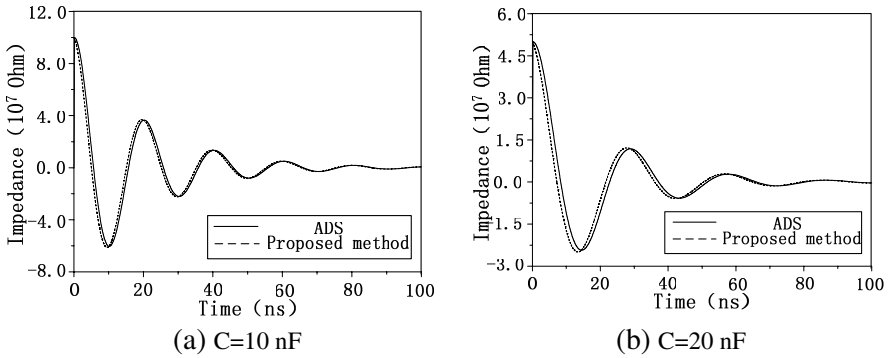
Figure 7. Time-domain impedance function waveforms of the PDN with different capacitance.

The damping characteristic of the circuit model is introduced by the resistor, so the real part of poles is unchanged due to the same resistance. The time-domain impedance function period is determined by the imaginary parts of poles, and the periods of $C = 10\,\text{nF}$ and $C = 20\,\text{nF}$ can be calculated as $20.1\,\text{ns}$ and $28.8\,\text{ns}$ with $T_{impedance} = 2\pi/p_{ni}$ respectively. The period of $C = 20\,\text{nF}$ is increased to $\sqrt{2}$ that of $C = 10\,\text{nF}$ due to the double capacitance, which is consistent with the resonant period of the circuit model, and Equation (27) is validated. From the aforementioned discussion, it is found that the characteristics of the time-domain impedance function are consistent with the frequency-domain impedance.

5. EXPERIMENTAL VALIDATIONS OF SIMULTANEOUS SWITCHING NOISE CALCULATION

5.1. Lumped Circuit Model of the Power Delivery Network

The lumped circuit model of a PDN is shown in Fig. 8, the pins of the package, PCB and VRM are modeled with series inductor and resistor. The parameters of capacitors for providing power to IC and parasitic parameters of pins are shown in this figure. The current source is a triangle current pulse that has an amplitude of $1\,\text{A}$ a rise/fall time of $0.1\,\text{ns}$, and a period of $2\,\text{ns}$, so the bandwidth of the frequency-domain impedance should be considered is $3.5\,\text{GHz}$. The simulated frequency-domain impedance of ADS is the same with that of Hspice, so the obtained frequency-domain impedance could be approximated with one same rational function, and the simulated and approximated results are shown in Fig. 9, they are consistent with each other, and the

0. 001   10nH
VRM=3.3v
0. 001
1nH
0.001
30pH
I
8n

0. 13n 0.13n 0.13n 0.13n 0.13n 0.13n
18. 8u 8.8u 4u 1.88u 0.88u 0.4u
4m 5m 6m 7m 6m 7.5m

0.1n 0.1n 0.1n 0.1n 0.1n
188n 80n 40n 18.8n 8.8n
10m 14m 19m 26m 53m

PCB   package   chip

Figure 8. Lumped circuit model of the PDN.

Table 1. Parameters of rational functions for different types of circuit models.

type	constant	pole	residue
lumped	1.97×10^{-6}	$-3.27 \times 10^{6} \pm \mathrm{j}\, 5.19 \times 10^{7}$	$1.33 \times 10^{6} \pm \mathrm{j}\, 1.30 \times 10^{5}$
		$-6.05 \times 10^{7} \pm \mathrm{j}\, 2.77 \times 10^{8}$	$2.93 \times 10^{5} \pm \mathrm{j}\, 4.66 \times 10^{4}$
		$-8.24 \times 10^{7} \pm \mathrm{j}\, 4.23 \times 10^{8}$	$5.46 \times 10^{5} \pm \mathrm{j}\, 1.52 \times 10^{5}$
		$-1.12 \times 10^{8} \pm \mathrm{j}\, 6.41 \times 10^{8}$	$9.00 \times 10^{5} \pm \mathrm{j}\, 2.76 \times 10^{5}$
		$-2.17 \times 10^{8} \pm \mathrm{j}\, 9.56 \times 10^{8}$	$1.30 \times 10^{6} \pm \mathrm{j}\, 1.57 \times 10^{6}$
		$-7.03 \times 10^{7} \pm \mathrm{j}\, 1.64 \times 10^{9}$	$5.81 \times 10^{7} \pm \mathrm{j}\, 3.88 \times 10^{6}$
distributed (ADS)	1.94×10^{-6}	$-9.55 \times 10^{6} \pm \mathrm{j}\, 8.05 \times 10^{7}$	$-2.18 \times 10^{5} \pm \mathrm{j}\, 3.82 \times 10^{5}$
		$-3.21 \times 10^{6} \pm \mathrm{j}\, 1.71 \times 10^{8}$	$2.45 \times 10^{7} \pm \mathrm{j}\, 4.52 \times 10^{6}$
		$-2.87 \times 10^{6} \pm \mathrm{j}\, 1.94 \times 10^{8}$	$2.50 \times 10^{7} \pm \mathrm{j}\, 5.23 \times 10^{6}$
		$-3.70 \times 10^{6} \pm \mathrm{j}\, 1.41 \times 10^{9}$	$2.89 \times 10^{5} \pm \mathrm{j}\, 2.35 \times 10^{5}$
		$-4.86 \times 10^{7} \pm \mathrm{j}\, 1.64 \times 10^{9}$	$3.50 \times 10^{5} \pm \mathrm{j}\, 8.03 \times 10^{4}$
distributed (Hspice)	1.21×10^{-6}	$-3.05 \times 10^{6} \pm \mathrm{j}\, 3.25 \times 10^{8}$	$9.65 \times 10^{7} \mp \mathrm{j}\, 5.26 \times 10^{3}$
		$-4.20 \times 10^{7} \pm \mathrm{j}\, 2.21 \times 10^{9}$	$3.03 \times 10^{6} \mp \mathrm{j}\, 1.72 \times 10^{5}$
		$-4.34 \times 10^{7} \pm \mathrm{j}\, 4.88 \times 10^{9}$	$3.81 \times 10^{4} \mp \mathrm{j}\, 9.86 \times 10^{2}$
		$-6.19 \times 10^{7} \pm \mathrm{j}\, 7.03 \times 10^{9}$	$1.82 \times 10^{5} \pm \mathrm{j}\, 7.85 \times 10^{2}$

parameters of the rational function are shown in Table 1. The main resonant period of the PDN is 3.8 ns and large enough compared to the width of switching current, so the switching current can be seen as impulse signal. The simulated SSN waveforms of ADS, Hspice and the proposed method are shown in Fig. 10, they have a good agreement, the proposed method is accurate for the lumped circuit model As shown in Table 2, the simulation time is reduced effectively compared with ADS and Hspice.
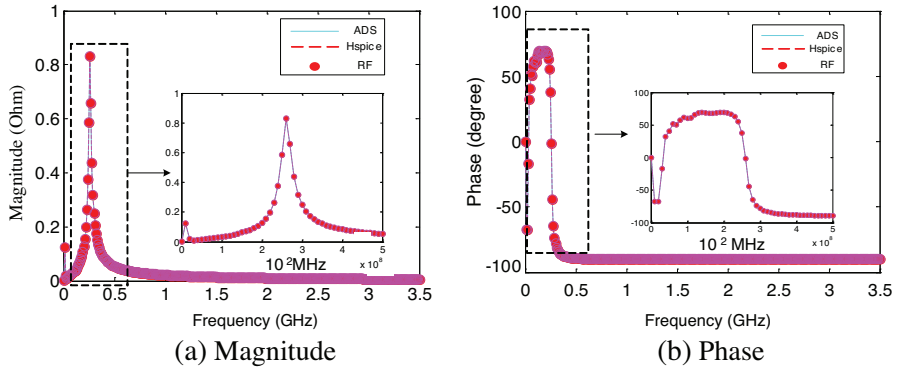
(a) Magnitude

(b) Phase

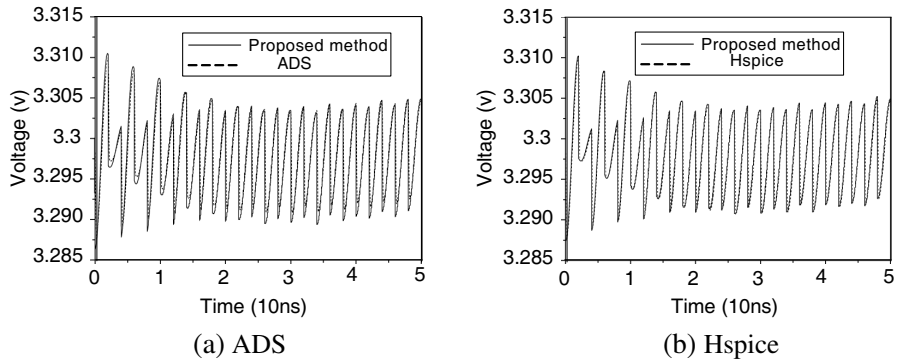**Figure 9.** Input impedance of the PDN.

(a) ADS
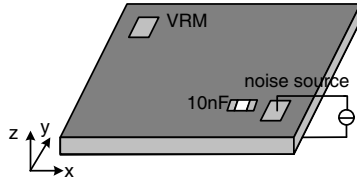
(b) Hspice

Figure 10. SSN waveforms of the PDN.

Table 2. Simulation time of SSN for different types of circuit models.

Type of model	Period of switching current	Method	Simulation time
Lumped	2 ns	ADS	2.34 s
		Hspice	1.03 s
		Proposed method	0.7 s
Distributed (ADS)	1 ns	ADS	20.7 s
		Proposed method	6.9 s
Distributed (Hspice)	2 ns	Hspice	15.4 s
		Proposed method	3.7 s

5.2. Distributed Circuit Model of the Printed Circuit Board

A distributed circuit model of a PCB with dimensions of $100\,\text{mm} \times 100\,\text{mm}$ is modeled in ADS and shown in Fig. 11, the noise source and VRM are located at $(90\,\text{mm}, 10\,\text{mm})$ and $(10\,\text{mm}, 90\,\text{mm})$ respectively. The DC voltage of VRM is 3.3 V, and the triangle current pulse source has an amplitude of 1 A, a rise/fall time of 0.1 ns, and a period of 1 ns, so the bandwidth of the frequency-domain impedance should be considered is 3.5 GHz. A 10 nF capacitor is placed close to the noise source for suppressing the noise transmission. The simulated frequency-domain impedance of ADS and the approximated results with the rational function are shown in Fig. 12, a good agreement is seen between them, and the parameters of the rational function are shown in Table 1. The main resonant period of the PDN is 33.3 ns and large enough compared to the width of switching current, so the switching current can be seen as impulse signal. The simulated SSN waveforms of ADS and the proposed method are shown in Fig. 13, they have the same noise period, and the largest magnitudes of noise are 0.062 V and 0.068 V respectively. As shown in Table 2, it needs less simulation time compared with ADS.

A distributed circuit model of a PCB with dimensions of $80\,\text{mm} \times$

Figure 11. Distributed circuit model of a PCB.
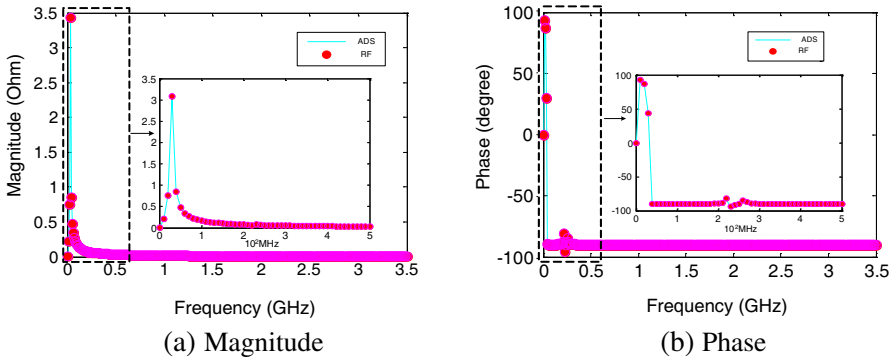
Figure 12. Input impedance of the PDN.

100 mm is modeled in Hspice and shown in Fig. 14, the noise source and VRM are located at (90 mm, 10 mm) and (10 mm, 70 mm) respectively. The DC voltage of VRM is 3.3 V, and switching current is a triangle current pulse that has an amplitude of 1 A a rise/fall time of 0.35 ns, and the period of switching current is fixed as 2 ns, so the bandwidth
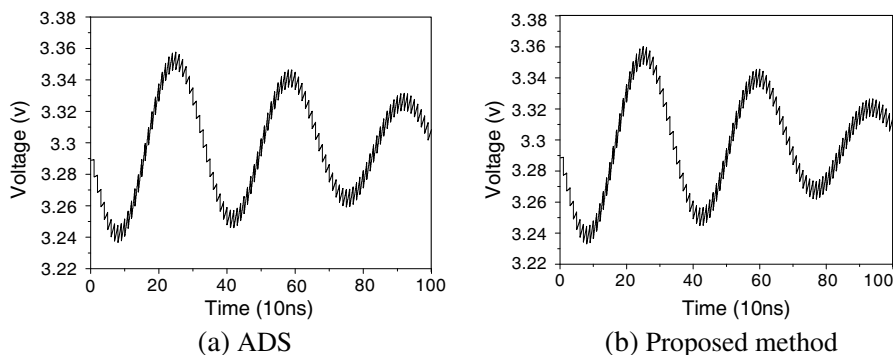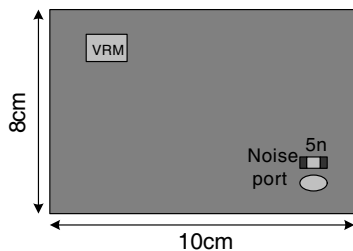

(a) ADS   (b) Proposed method

Figure 13. SSN waveforms of the PDN.
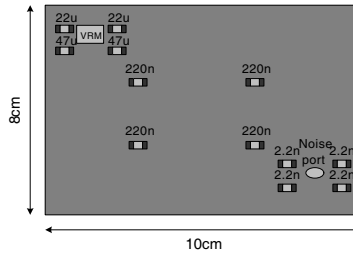

Figure 14. Distributed circuit model of a PCB.

(a) Magnitude   (b) Phase
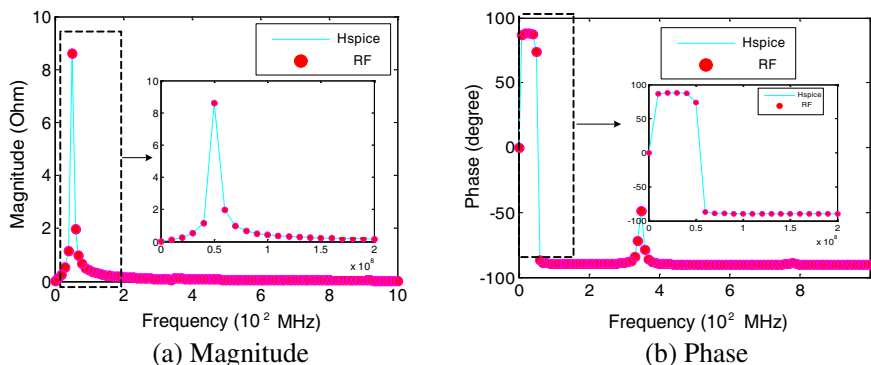
Figure 15. Input impedance of the PDN.

(a) Hspice   (b) Proposed method
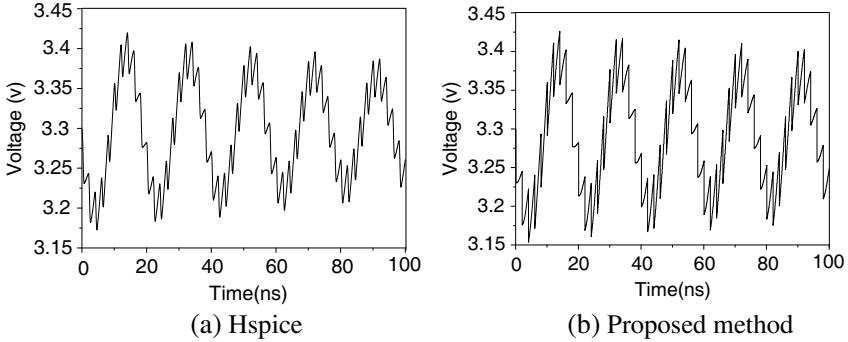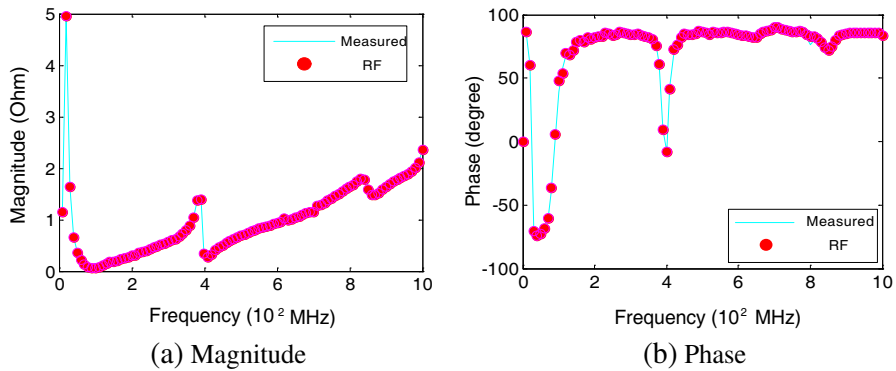
Figure 16. SSN waveforms of the PDN.

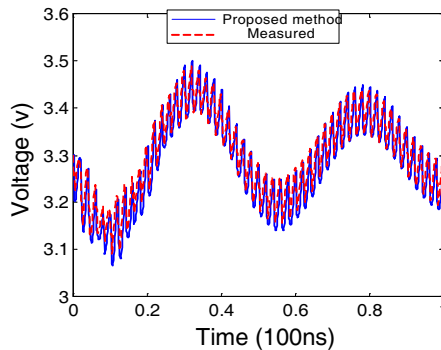**Figure 17.** Placement of decoupling capacitors.

of the frequency-domain impedance should be considered is 1 GHz. A 5 nF capacitor is placed close to the noise source for suppressing the noise transmission. The simulated frequency-domain impedance of Hspice and the approximated results with the rational function are shown in Fig. 15, and the parameters of the rational function are shown in Table 1. The main resonant period of the PDN is 20 ns, so the switching current can be seen as impulse signal. The simulated SSN waveforms of Hspice and the proposed method are shown in Fig. 16, they have the same noise period, and the largest magnitudes of noise are 0.125 V and 0.15 V respectively. So the proposed method is accurate for the distributed circuit model, and as shown in Table 2, it needs less simulation time compared with Hspice.

5.3. Measurement Verification

A PCB with dimensions of 100 mm × 80 mm is built and shown in Fig. 17, the noise port and VRM are located at (90 mm, 10 mm) and (10 mm, 70 mm) respectively. The DC voltage of VRM is 3.3 V, the triangle current pulse source that has an amplitude of 1 A a rise/fall time of 0.35 ns, and a period of 2 ns is launched at the noise port. So the

(a) Magnitude

(b) Phase

Figure 18. Measured input impedance and approximated results of the PDN.

Figure 19. SSN waveforms of the PDN.

bandwidth of the frequency-domain impedance should be considered is $1\,\text{GHz}$. Two $47\,\mu\text{F}$ capacitors with $ESR = 12\,\text{m}\Omega$, $ESL = 1.4\,\text{nH}$, two $22\,\mu\text{F}$ capacitors with $ESR = 14\,\text{m}\Omega$, $ESL = 1.4\,\text{nH}$ are placed close to the VRM, four $220\,\text{nF}$ capacitors with $ESR = 23\,\text{m}\Omega$, $ESL = 0.5\,\text{nH}$ are placed on the PCB dispersedly, they are treated as global decoupling capacitors. Four $2.2\,\text{nF}$ capacitors with $ESR = 221\,\text{m}\Omega$, $ESL = 0.4\,\text{nH}$ are placed close to the noise port and treated as local decoupling capacitors. The frequency-domain impedance was measured using an Agilent HP8753E Network Analyzer and calibration procedure (Short-Open-Load-Through, SOLT) was performed. The measured results and approximated results with the 80 poles and residues are shown in Fig. 18. The main resonant period is $50\,\text{ns}$, so the switching current can be seen as impulse signal compared to the width of switching current. The noise voltage of noise port was measured using a Tektronix TDS5104B two-channel digitizing oscilloscope. The

simulated and measured SSN waveforms are shown in Fig. 19, they have the same noise period and the largest magnitudes of noise are 0.23 V and 0.21 V respectively, a good agreement is achieved.

## 6. ANALYSIS OF THE SIMULTANEOUS SWITCHING NOISE SUPPRESSION

It is found that the time-domain impedance function represents periodic characteristics, whose period is mainly determined by the imaginary part of pole with the largest $\sqrt{\left(k_{nr}^2 + k_{ni}^2\right)}$. The SSN is periodic accumulation of the time-domain impedance waveform based on the period of switching current, so the magnitude of SSN would accumulate in phase with $T_{current} = (n + 1) T_{impedance}$, $(n = N)$, and the magnitude of SSN would accumulate out phase with $T_{current} = (n + 1/2) T_{impedance}$, $(n = N)$, so SSN could be suppressed through changing the period of switching current and time-domain impedance function.

As shown in Fig. 8, the time-domain impedance function period can be calculated as 3.73 ns. Switching current is a triangle current pulse that has an amplitude of 1 A, a rise/fall time of 0.1 ns, and a period of variable parameter T. The simulated SSN waveforms of ADS with $T = 3.73$ ns and $T = 1.81$ ns are shown in Fig. 20. For $T = 3.73$ ns, the period of switching current is the same with the time-domain impedance function, noise would be increased in phase, the magnitude is 0.041 V, and for $T = 1.87$ ns, the period of switching current is half of the time-domain impedance function, noise would be reduced out phase, the magnitude is 0.012 V, though switching current of $T = 1.87$ ns has higher current density and power, less SSN is produced. It is concluded that the SSN can be suppressed effectively by adjusting the period of switching current based on the period of time-domain impedance function.

For fixed period of switching current, SSN can also be suppressed by adjusting the period of time-domain impedance function. As shown in Fig. 8, switching current is a triangle current pulse that has an amplitude of 1 A a rise/fall time of 0.1 ns, and the period of switching current is fixed as 3 ns. The inductance of package pins is increased from 30 pH to 90 pH, and the period of the time-domain impedance function is changed to 6 ns, which is 2 times period of switching current, so the magnitude of SSN would accumulate out phase. The simulated SSN waveforms of ADS are shown in Fig. 21, it is found that the SSN of 90 pH is suppressed effectively and the largest magnitudes of 30 pH and 90 pH are 0.0167 V and 0.0125 V respectively. The simulated

(a) T=3.73ns

(b) T=1.87ns
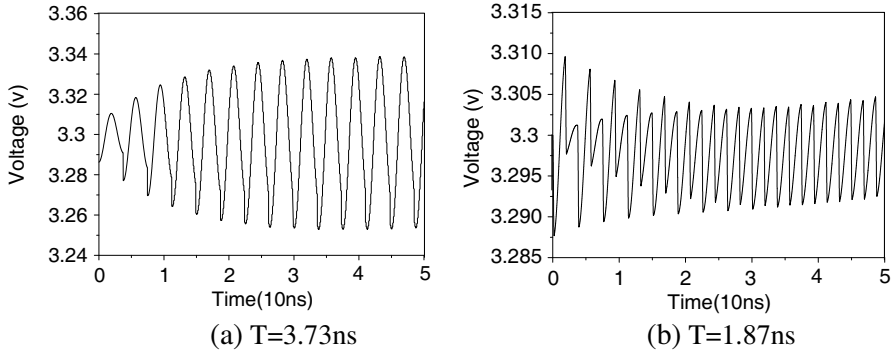
Figure 20. SSN waveforms of different switching current periods.

(a) L $_{package}$ =30 pH

(b) L $_{package}$ =90 pH
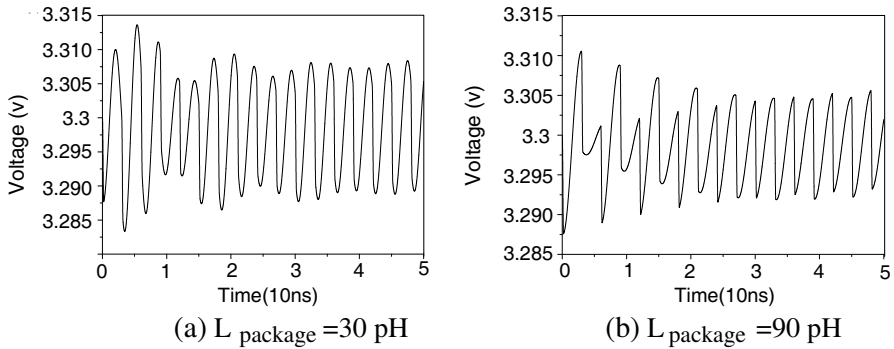
Figure 21. SSN waveforms of different time-domain impedance periods.

SSN of 90 pH is less than that of 30 pH, though the package pin has larger inductance. It is important to note that the period of the time-domain impedance function could also be changed through adjusting capacitance for the SSN suppression, and the magnitude of the time-domain impedance function can be reduced by larger capacitance and smaller inductance, which results in less SSN.

7. CONCLUSION

In this paper, a new method is proposed to calculate and suppress the SSN with the time-domain impedance function of the PDN which is obtained by approximating the impedance frequency response of the PDN with the rational function based on switching current characteristics in time domain. The time-domain impedance function is discussed in details, and it is found that the SSN can be

suppressed by adjusting the period of switching current and time-domain impedance function, because SSN is periodic accumulation of time-domain impedance waveform based on the period of switching current. The performance of the new method for calculating and suppressing the SSN is verified with lumped, distributed PDN models and measured results.

ACKNOWLEDGMENT

REFERENCES

1. Hsu, H.-S. and H.-T. Hsu, "System level integration of simulation methods for high data-rate transmission circuit design applications," *Progress In Electromagnetics Research*, Vol. 90, 31–49, 2009.

2. Xu, K., Z. Fan, D.-Z. Ding, and R.-S. Chen, "Gpu accelerated unconditionally stable crank-nicolson FDTD method for the analysis of three-dimensional microwave circuits," *Progress In Electromagnetics Research*, Vol. 102, 381–395, 2010.

3. Tahir, F. A., H. Aubert, and E. Girard, "Equivalent electrical circuit for designing mems-controlled reflectarray phase shifters," *Progress In Electromagnetics Research*, Vol. 100, 1–12, 2010.

4. Y. Liu, L. Tong, Y. Tian, and B. Gao, "Measurements of planar microwave circuits using an improved Trl calibration method," *Progress In Electromagnetics Research*, Vol. 109, 263–278, 2010.

5. Meng, Y. S., Y. H. Lee, and B. C. Ng, "Further study of rainfall effect on VHF forested radio-wave propagation with four-layered model," *Progress In Electromagnetics Research*, Vol. 99, 149–161, 2009.

6. Qian, Z.-G., M.-S. Tong, and W. C. Chew, "Conductive medium modeling with an augmented GIBC formulation," *Progress In Electromagnetics Research*, Vol. 99, 261–272, 2009.

7. Wu, B. and L. Tsang, "Full-wave modeling of multiple vias using differential signaling and shared antipad in multilayered high speed vertical interconnects," *Progress In Electromagnetics Research*, Vol. 97, 129–139, 2009.

8. Lin, Z., X. Zhang, and G. Fang "Theoretical model of electromagnetic scattering from 3D multi-layer dielectric media with slightly rough surfaces," *Progress In Electromagnetics Research*, Vol. 96, 37–62, 2009.

9. Parise, M. and S. Cristina, "High-order electromagnetic modeling of shortwave inductive diathermy effects," *Progress In Electromagnetics Research*, Vol. 92, 235–253, 2009.

10. Zhang, J., M. Y. Koledintseva, G. Antonini, J. L. Drewniak, A. Orlandi, and K. N. Rozanov, "Planar transmission line method for characterization of printed circuit board dielectrics," *Progress In Electromagnetics Research*, Vol. 102, 267–286, 2010.

11. Xie, H., J. Wang, R. Fan, and Y. Liu, "Study of loss effect of transmission lines and validity of a spice model in electromagnetic topology," *Progress In Electromagnetics Research*, Vol. 90, 89–103, 2009.

12. Wang, Z., W. Che, and L. Zhou, "Uncertainty analysis of the rational function model used in the complex permittivity measurement of biological tissues using PMCT probes within a wide microwave frequency band," *Progress In Electromagnetics Research*, Vol. 90, 137–150, 2009.

13. Zhang, P.-F., S.-X. Gong, and S. F. Zhao, "Fast hybrid FEM/CRE-UTD method to compute the radiation pattern of antennas on large carriers," *Progress In Electromagnetics Research*, Vol. 89, 75–84, 2009.

14. Torkaman, H. and E. Afjei, "FEM analysis of angular misalignment fault in SRM magnetostatic characteristics," *Progress In Electromagnetics Research*, Vol. 104, 31–48, 2010.

15. Liu, Y. H., Q. H. Liu, and Z.-P. Nie, "A new efficient FDTD time-to-frequency-domain conversion algorithm," *Progress In Electromagnetics Research*, Vol. 92, 33–46, 2009.

16. Manzanares-Martinez, J. and P. Castro-Garay, "Modeling the tuning of lasing in liquid crystal based one-dimensional photonic-crystals using the Finite Difference Time-Domain method," *Journal of Electromagnetic Waves and Applications*, Vol. 24, No. 14–15, 1867–1875, 2010.

17. Swillam, M. A., R. H. Gohary, M. H. Bakr, and X. Li, "Efficient approach for sensitivity analysis of lossy and leaky structures using FDTD," *Progress In Electromagnetics Research*, Vol. 94, 197–212, 2009.

18. Kim, H., Y. Jeong, J. Park, S. Lee, J. Hong, and Y. Hong, "Significant reduction of power/ground inductive impedance and simultaneous switching noise by using embedded film capacitor," *Electr. Perform. Electron. Package*, 129–132, 2003.

19. Hobbs, J. M., H. Windlass, V. Sundaram, S. Chun, G. E. White, M. Swaminathan, and R. R. Tummala, "Simultaneous switching noise suppression for high speed systems using embedded

decoupling," *Proceeding Electron. Comon. Technol. Conference*, 339–343, 2001.

20. Hubing, T., J. Chen, J. Drewnik, T. V. Doren, Y. Ren, J. Fan, and R. E. DuBroff, "Power bus noise reduction using power island in printed circuit board designs," *Proc. Int. Symp. Electromagn. Compat. 1999*, 1–4, 1999.

21. Wu, T. L., S. T. Chen, J. N. Huang, and Y. H. Lin, "Numerical and experimental investigation of radiation caused by the switching noise on the partitioned dc power/ground-planes of high-speed digital PCB," *IEEE Trans. Electromagnetic Compatibility*, Vol. 46, 33–45, 2004.

22. Zeeff, T. M. and T. H. Hubing, "Reducing power bus impedance at resonance with lossy components," *IEEE Trans. Advanced Package*, Vol. 25, 307–310, 2002.

23. He, Y., L. Li, C. H. Liang, and Q. H. Liu, "EBG structureswith fractal topologies for ultra-wideband ground bounce noisesuppression," *Journal of Electromagnetic Waves and Applications*, Vol. 24, No. 10, 1365–1374, 2010.

24. Masri, T., M. K. A. Rahim, H. A. Majid, O. Ayop, F. Zubir, and M. N. A. Karim, "Electromagnetic band gap structure for planarultra wide band antenna," *Journal of Electromagnetic Waves and Applications*, Vol. 24, No. 2–3, 229–239, 2010.

25. Smith, L. D., R. E. Anderson, D. W. Forehand, T. J. Pelc, and T. Roy, "Power distribution system design methodology and capacitor selection for modern CMOS technology," *IEEE Trans. Advanced Package*, Vol. 22, 284–291, 1999.

26. Faghihi, F. and H. Heydari, "Time domain physical optics for the higher-order FDTD modeling in electromagnetic scattering from 3-D complex and combined Multiple Materials Objects," *Progress In Electromagnetics Research*, Vol. 95, 87–102, 2009.

27. Drewniak, J. L., et al., "Comparing time-domain and frequency domain techniques for investigation on charge delivery and power-bus noise for high-speed printed circuit boards," *DesignCon*, 2007.

28. Cheng, W. L., A. Sarkar, S. Lin, and J. Zheng "Worst case switching pattern for core noise analysis," *DesignCon*, 2009.

29. Gustavsen, B. and A. Semlyen, "Rational approximation of frequency response by vector fitting," *IEEE Power Delivery*, Vol. 14, 1052–1061, 1999.

30. Eric, B., *Signal Integrity-simplified*, Prentice Hall PTR, 59–61, 2003.